OPTIMAL PASSIVE DAMPER PLACEMENT METHODOLOGY FOR INTERFEROMETERS USING INTEGRATED STRUCTURES/OPTICS MODELING'

Sanjay S. Joshi,[2] Mark M. Milman,[3] and James W. Melody[4]
Jet Propulsion Laboratory
California Institute of Technology
Pasadena, California 91109

ABSTRACT

Interferometers collect the light from stars at two different points in space using telescopes or mirrors (apertures). They then direct this light to a common point to produce interference fringes. A crucial requirement for this system is that the distance the light travels from one aperture to the interference point, called the optical pathlength, must match the distance the light travels from the other aperture to the interference point to within a few nanometers. The difference in optical pathlengths is called optical path difference (OPD). Clearly, with any type of structural disturbance, such as that caused by attitude control actuators, the nanometer requirement will not be met due to structural vibration. The fundamental approach to meeting this requirement involves three vibration attenuation *layers:* vibration isolation, structural quieting, and active optics. The strategy is to isolate vibrating machinery at the point of attachment, to add damping to the structure, and finally, to actively control certain optical components in order to reach the requirement. This paper focuses specifically on passive structural damping with the goal to lower the control demand on active optics. In order to develop a methodology for passive damper placement for interferometers, several analytical tools must be integrated. These are (1) an integrated structural/optics interferometer model, (2) passive damper models, (3) damper placement strategy, and (4) optimization metric analysis. In this paper, we discuss each of these analytical tools by applying them to a representative interferometer. The goal is to suppress *errors* in OPD caused by random noise disturbances on one point of the structure. An integrated structures/optics model is created of an interferometer. Since an unlimited number of dampers is infeasible and a large number of possible damper positions exist, we explore the use of combinatorial optimization of damper locations. *In* particular, simulated annealing optimization is chosen as a way to optimise over *several* local minima.

[2]Staff Engineer. Member AIAA. Corresponding Author: JPL Mail stop 19S-326, Phone: (818) 354-0541 Email: sanjay.s.joshi@jpl.nasa.gov

[3]Senior Engineer.

[4]Staff Engineer.

1 INTRODUCTION

Both NASA and the European Space Agency are currently studying the feasibility of placing large baseline *in*terferometers in space to perform detailed astrometric measurements and also to image distant solar systems. Interferometers collect light from stars at two different points in space using telescopes or mirrors (apertures). They then direct this light to a common point to produce interference fringes. The visibility of these fringes provides information that allows astrometry and imaging. A crucial requirement for this system is that the distance the light travels from one aperture to the interference point, called the optical pathlength, must match the distance the light travels from the other aperture to the interference point to within a few nanometers (1×10^{-9} meters) . The difference in optical pathlengths is called optical path difference (OPD). Many interferometer designs studied to date place the two collecting apertures on either end of a long flexible structure. Clearly, with any type of structural disturbance, such as that caused by attitude control actuators, the nanometer requirement will not be met due to structural vibration.

The NASA Interferometry Technology Program evolved from a system design for the Focused Mission Interferom*eter* (FMI): a space-based, 30m baseline, partial aperture

telescope concept [Laskin & San Martin (1989)]. Using analytical models of the spacecraft and the disturbance environment, this effort predicted 1 micron (RMS) on-orbit fringe position motion in the unattenuated spacecraft environment. This fringe motion is a factor of 100 above the required level of 10 nm (RMS). This discrepancy inspired the layered vibration attenuation strategy. Figure 1 presents the fundamental approach in terms of the three vibration attenuation layers: vibration isolation, structural quieting, and active optics. The strategy is to isolate vibrating machinery at the point of attachment, to add damping to the structure, and finally, to actively control certain optical components in order to reach the 10 nm requirement.

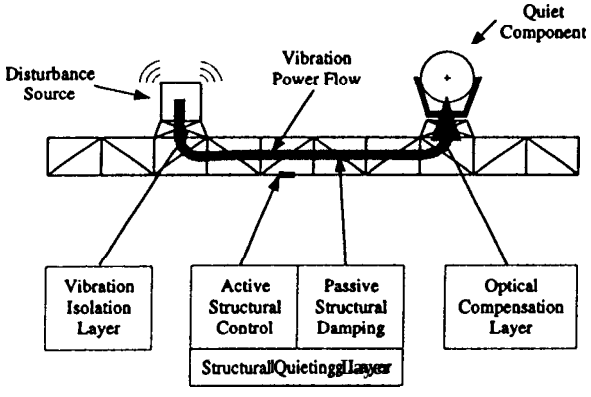

Figure 1. Interferometry Technology Program's layered control approach.

Several papers have addressed issues of structural isolation and active optical control for interferometers [Melody & Neat (1997)] [Spanos, et. al. (1995)]. This paper focuses specifically on passive structural damping with the goal to lower the control demand on active optics. In order to carry out a study on structural damping for interferometers, several analytical tools must be integrated. These are (1) an integrated structural/optics interferometer model, (2) passive damper models, (3) damper placement strategy, and (4) optimization metric analysis. In this paper, we discuss each of these analytical tools by applying them to a representative interferometer . The goal is to suppress errors in OPD caused by random noise disturbances on one point of the structure. For this purpose, an integrated structures/optics model is created of an interferometer. Since an unlimited number of dampers is infeasible and a large number of possible damper positions exist, we explore the use of combinatorial optimization of damper locations. In particular, simulated annealing optimization is chosen as a way to optimize over several local minima.

2 INTERFEROMETER MODEL

A finite element model of a representative two-truss interferometer structure was created using the Integrated Modeling of Optical Systems (IMOS) tool developed at J PL. IMOS allows finite element models of structures to be built with integrated optics attached. This model was based on a previous interferometer model described in [Melody (1996)]. It models a free-flying, 10 meter baseline, dual-star feed interferometer. The model includes two trusses on which the collecting apertures are mounted, a rigid central bus node modeled after the NASA Space Shuttle ASTRO-SPAS carrier, and attachment points for the optical elements. The ASTRO-SPAS node is connected to an optics node via a rigid body element. The two trusses are composed of six-degree-of-freedom beam elements. The ASTRO-SPAS node is connected to the trusses by four rigid body elements to each of the four corners of each truss. The geometry of the interferometer structure is shown in figure 2. The length of each truss is 4 meters. It is partitioned into

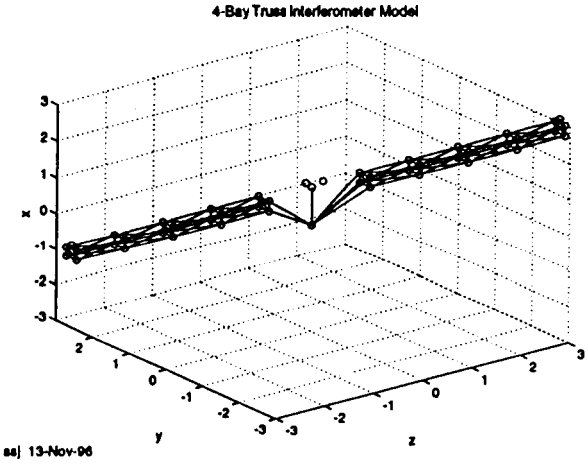

Figure 2. A two-truss interferometer based on ISIS [1].

4 one meter long bays. The cross section of each bay is 0.28 x 0.28 m^2. Each truss is composed of 57 beam elements [Milman (1995)]. The first four non rigid-body modes of the interferometer structure are shown in figure 3.

From the double truss interferometer model, standard mass and stiffness matrices associated with a finite-element model were obtained,

$$M\frac{d^2x}{dt^2} + Kx = F \qquad (1)$$

The model contained 408 degrees of freedom in physical space. This resulted in physical mass, M, and stiffness, K,

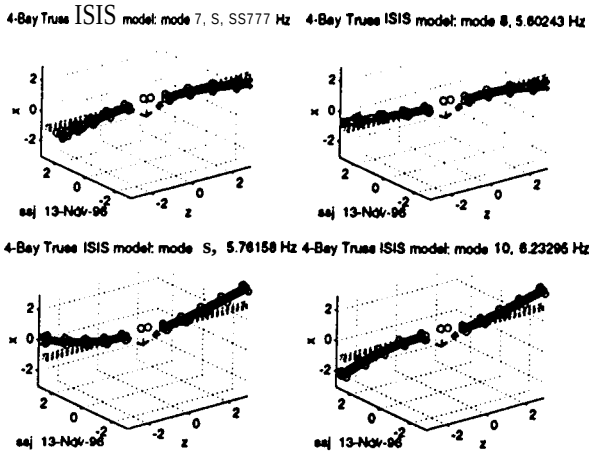

Figure 3. First four non-rigid modes of double truss interferometer.

matrices of size [408 x 408]. Of the 408 degreea of freedom, several were dependent **DOF's**. The dependent degrees of freedom resulted from rigid body element connections. After removing these dependent degrees of freedom, 162 degrees of freedom remained, resulting in reduced mass and stiffness matrices, M_r and K_r, of [162 x 162]. This size model was still too large to be analyzed repeatedly. As a result, a modal transformation was made to lower dimensional space for analysis of modal frequencies and damping. The transformation matrix, T [162 x 50], was composed of 50 eigenvectors, ν, of $M_r^{-1}K_r$.

$$T \triangleq [\nu_1, \nu_2, \ldots \nu_{50}] \tag{2}$$

A reduced order system was then produced aa

$$z \triangleq Ty; \qquad T^t M T \frac{d^2y}{dt^2} + T^t K T y = T^t F \tag{3}$$

where the superscript t refers to a matrix transpose. The new matrices, $\overline{M} \triangleq T^t M T$ and $\overline{K} \triangleq T^t K T$, are of size [50 x 50] and $\overline{F} \triangleq T'F$ is of size [50 x 1].

3 PASSIVE DAMPERS

Passive dampers were incorporated in the FEM model as viscous dampers based on the **Honeywell 'D-strut' [Neat, et. al. (1992)].** A viscous damping force is created along the axial direction that is proportional to the axial displacement rate of the beam element. In this article, it is assumed that the new passive damping element and the original beam element have the same stiffness. A new model with a passive damping element, denoted by the subscript i, is written as (in physical space)

$$M\frac{d^2x}{dt^2} + (K + \delta K_i)x = Fu + D_i d_i \quad i = 1 \ldots \quad N \tag{4}$$

where D_i is the influence vector associated with an axial force between two nodes of the structure, d_i is a damper actuator force aa in [Chu & Milman (1992)], and δK_i is the change in stiffness associated with the change in elastic modulus of the damper beam element. Recall in this report, $\delta K \triangleq$ O. The force d_i is modeled as a linear velocity feedback so

$$d_i = -k_w v_i \qquad v_i = D^T \frac{dx}{dt} \tag{5}$$

where k_w is a scalar used to change the value of damping. By substituting (5) into (4), we obtain a damping matrix, C,

$$M\frac{d2z}{dt^2} + (k_w D_i D_i^t)\frac{dx}{dt} + (K + \delta K_i)x = Fu \tag{6}$$

where $C \triangleq k_w D_i D_i^t$.

4 STATE SPACE REPRESENTATION

In this section, we create a state space model of a disturbance input to the ASTRO-SPAS node and a measurement output of optical path difference (OPD). The ASTRO-SPAS node is the most likely place of structural disturbance since it is the place where attitude control system actuators such as thrusters will be placed.

The reduced order dynamic system with viscous damping is represented as

$$\overline{M}\frac{d^2y}{dt^2} + \overline{C}\frac{dy}{dt} + \overline{K}y = \overline{F}u \tag{7}$$

where $\overline{M}$ is the reduced mass matrix, $\overline{C}$ is the reduced damping matrix, $\overline{K}$ is the reduced stiffness matrix, and $\overline{F}$ is the reduced disturbance influence vector for the ASTRO-SPAS node. By denoting a new state, p, as

$$p \triangleq \begin{bmatrix} y \\ \frac{dy}{dt} \end{bmatrix}, \tag{8}$$

(7) may be written in state variable form as

$$\frac{dp}{dt} = \begin{pmatrix} 0 & I \\ -M^{-1}K & -M^{-1}C \end{pmatrix} p + \begin{bmatrix} 0 \\ M^{-1}F \end{bmatrix} u \qquad (9)$$

The quantity of interest is the optical pathlength difference (OPD). The transformation matrix, H, that takes the red uced order displacement vector, y, to the OPD is created using the Controlled Optics Modeling Package (COMP) [Redding (1992)]. This is represented as

$$OPD = [H\ 0]\, p \qquad (10)$$

The H matrix is based on a sensitivity analysis of the optical pathlength with respect to the change in optical mounting positions and orientations. A nominal light ray trace from collecting apertures to the interference point is shown in figure 4. Before arriving at the interference point, light rays trace a path through several optical elements including siderostats, beam compressors, and steering mirrors. Rewrite (9) and (10) as

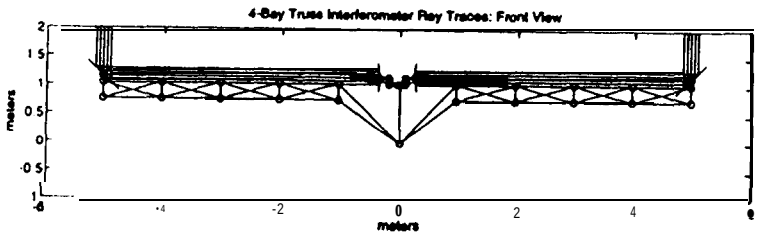

Figure 4. Nominal ray trace from apertures to interference point.

$$\frac{dp}{dt} = \tilde{A}p + \tilde{B}u \qquad (11)$$

$$OPD = \tilde{C}p \qquad (12)$$

where the definitions of $\tilde{A}$, $\tilde{B}$, and $\tilde{C}$ are clear.

5 OPTIMIZATION FOR DAMPER PLACEMENT

Since an unlimited number of dampers is infeasible and a large number of possible damper locations exist, we explore the use of combinatorial optimization of damper locations.

5.1 Optimization Metric

Let the system input, u(t), be a Gaussian, white noise force input with *zero* mean and standard deviation, $\sigma_\nu = 1$ Newton. This is meant to simulate a very general disturbance input. Specific sources of disturbances, such as reaction wheels [Hasha (1986)], have particular power spectral densities that may be realized as white noise through a linear filter. This filter can be then incorporated into the state space description of the system (11). As a result of the Gaussian input, the output OPD is also a zero mean Gaussian process. (A Gaussian random variable through a linear filter is Gaussian.) The steady state variance of OPD, σ^2_{OPD}, is related to the steady state variance of the white, Gaussian noise input, σ^2_ν, as

$$\sigma^2_{OPD} = \tilde{C}Q\tilde{C}^* \qquad (13)$$

where Q is the solution to the Lyapunov equation

$$Q\tilde{A} + \tilde{A}^*Q = -\tilde{B}\sigma^2_\nu\tilde{B}^* \qquad (14)$$

This becomes a scalar measure of the disturbance transmission from input to output. The damper placement objective becomes

$$\min_{DamperLocation} [\sigma_{OPD}] \qquad (15)$$

for a given $\sigma_\nu = 1$ Newton.

5.2 Simulated Annealing Optimization

Since the number of possible combinations for damper placement is prohibitively large, global optimization is infeasible. Therefore, we use a heuristic simulated annealing technique for optimization. Simulated annealing haa previously been used in general case damper placement problems in [Chu & Milman (1992)] and [Chen, et. al. (1991)]. Most common combinatorial optimization routines follow an iterative improvement strategy in which a trial solution cost is compared to the previous low combination cost. If the new cost is lower, then the trial solution is deemed the new low-cost combination. This method will find a local minima, but has the disadvantage of being stuck in a particular

local minima even though other local minima may provide a lower overall cost. The simulated annealing strategy differs in that is occasionally accepts a trial solution as the new low-cost solution even though the new cost has actually increased. This occasional acceptance of a non-improving trial combination allows the current solution to jump to other local minima. The probability of accepting a non-improving solution is governed by a so called Boltzmann probability function

$$P = e^{-\Delta E/\theta} \tag{16}$$

where AE is the change in cost from the previous low-cost combination and θ is a free-parameter known as the pseudo-temperature. θ is slowly decreased as the algorithm proceeds. It is to be noted that as the temperature decreases, the probability of accepting a non-improving solution also decreases. This forms a convergence pattern shown in figure 6 in which initially many non-improving solutions are accepted resulting in increased overall cost, but eventually the search settles to a particular local minima region where only lower cost combinations are accepted. Note also that large increases in energy (large positive AE), prohibit the acceptance of a non-improving trial combination. In the IMOS simulated annealing routine, a new trial combination is created by perturbing one element in the current low-cost combination. The element which is perturbed is selected by a uniform random number generator. This element is changed to a random value in the space of all possible damper locations again by a uniform random number generator.

6 RESULTS

6.1 Vibration Attenuation Results

In order to compare results, a nominal model was created by assuming zero dampers and .l% damping in all modes of the model. This value was used aa a reference in order to express performance in *dB*.

$$dB \triangleq 20 log_{10} \left(\frac{\sigma_{OPD}^{WithDampers}}{\sigma_{OPD}^{NoDampers}} \right) \tag{17}$$

Note that σ_{OPD} with any number of dampers will be less than σ_{OPD} with *zero* dampers. Therefore, in terms of dB defined above, better performance will have a more negative dB value. Figure 5 shows the results. All dampers have a value, k_w, of 7.005 x 10^4Ns/m . This value is representative

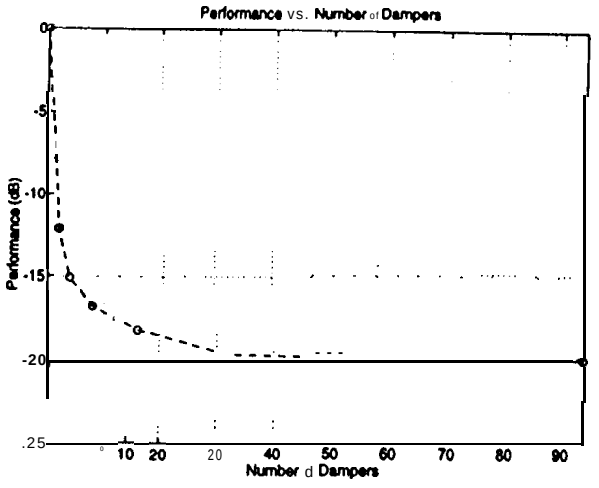

Figure 5. Performance vs. number of dampers. Circles represent calculated data points.

of the values of the Honeywell dampers built for previous structures work done at JPL [Neat, et. al. (1992)]. The maximum number of damper locations is 94. Therefore, the performance value at 94 dampers of –20. $10dB$ forms a floor for the performance function. This indicates that an order of magnitude improvement in vibration attenuation could be achieved using these dampers. The minimum number of damper locations is O. Therefore, the performance value of $0dB$ forms a ceiling for the performance function. We see that by placing dampers at optimal locations, we obtain significant performance value by using only a few dampers. Indeed, by using only 2 dampers, we obtain over half of the maximum performance available. This result becomes clear when we examine actual damper locations.

6.2 Four Damper Placement

Figures 6 shows a representative simulated annealing optimization run for the optimal placement of four dampers, each with k_w = 7.005x 10^4Ns/m . In addition, .1% modal damping is assumed in the model. An initial damper combination is chosen at random. Figure 7 shows the initial and final damper locations as a result of the optimization. The dampers tend to migrate to the base of the trusses. This indicates that dampers are placed at points of high axial stress of low modes.

7 EFFECT OF VIBRATION ISOLATION

It has been shown [Spanos, et. al. (1995)] that vibration isolation tends to act as a low-pass filter. Therefore, we may adjoin a low-pass filter to our model to study damper placement in the presence of vibration isolation (to first or-

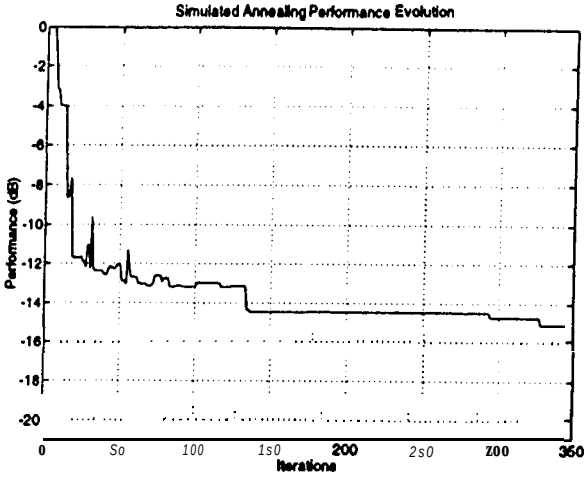

Figure 6. Simulated annealing convergence for four damper placement.

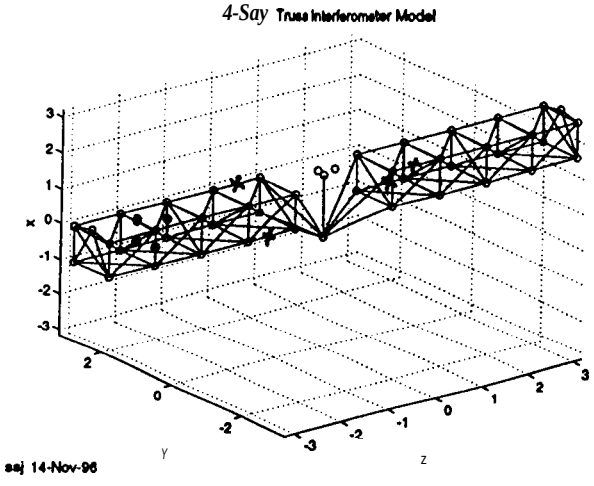

Figure 7. Four damper placement optimization. Initial damper locations are shown as closed circles. Final damper locations are shown as stars. Note that the interferometer is not drawn to actual dimension as in figure 2 in order to more clearly show damper positions.

der). A low-pass chebyshev filter with cut-off frequency of 10 Hz was appended to the input of the model. Results of the analysis were extremely similar to those results in the previous section. This indicates that in this case, the damper placement works most on low modes whose effect is not curtailed by the low-pass "isolation" filter.

8 CONCLUSIONS AND FUTURE WORK

Damper optimization has been explored for interferometer structures. An intergrated structures/optics model haa been created. Using a particular scalar disturbance rejection performance metric, consisting of the standard deviation of OPD as a result of noise input at the interferometer base, it was shown damper placement can significantly reduce OPD error. Simulated annealing optimization was used to optimize the placement of a finite number of dampers. It was shown that a small number of dampers give significant performance enhancement. Optimal damper placement tended to place dampers near the base of the interferometer trusses. This result indicates that dampers are placed at locations of high axial stress of low modes. For future interferometer structures that contain several trusses and several disturbance sources, this methodology should provide valuable information for analysis of passive damper placement.

Future work involves producing this analysis for the Micro-Precision Interferometer teatbed models [Melody & Neat (1997)] and then physically implementing passive damping on the testbed.

ACKNOWLEDGMENT

We are pleased to acknowledge Dr. Gregory W. Neat of JPL for many helpful discussions and suggestions.

This work was performed at the Jet Propulsion Laboratory, California Institute of Technology, under contract with the National Aeronautics and Space Administration.

REFERENCES

Melody, J. W., "ISIS Integrated Model and RCS Thruster Disturbance Analysis," *JPL Inter-o#ice Memorandum 341-96-174 ITP (Internal Document)* , May 20, 1996.

Chu, C.-C. and Milman, M. H., "Eigenvalue Error Analysis of Viscously Damped Structures Using a Ritz Reduction Method," *AIAA Journal,* December, 1992.

Milman, M.H. and C.-C. Chu, "Optimization Methods for Passive Damper Placement and Tuning," *Journal of Guidante, Control, and Dynamics,* July-August, 1994.

Chen, G.-S., Bruno, R. J., and Salama, M., "optimal Placement of Active/Passive Members in Truss Structures Using Simulated Annealing," *AIAA Journal,* August, 1991.

Neat, G. W., O'Brien J. F., Lurie, B. J., and Garnica, A., "Joint Langley Research Center/ J PL CSI Experiment," *15th Annual AAS Guidance and Control Conference,* February 8-12, 1992.

Milman, M. (cd.), "Integrated Modeling of Optical Systems User's Manual: Release 2.0," J PL D-13040 (Internal Document), November 15, 1995.

Redding, D., Needels, L., Wallace, K., and Levine, M., "Controlled Optics Modelling Package User Manual," JPL D-9816 (Internal Document), June 1, 1992.

LaSkin, R. A. and San Martin, M., "Control Structure System Design of a Spaceborne Interferometer," *Proceedings of the AA S/AIAA Astrodynamics Specialist Conference,* Stowe, VT, 1989.

Spanos, J.T., Rahman, Z., and Blackwood, G., "A Soft 6-Axis Active Vibration Isolator," *American Control Conference,* pp. 412-416, Seattle, WA, June, 1995.

J. W. Melody, G. W. Neat, "Integrated Modeling Methodology Validation Using the Micro-Precision Interferometer Testbed: Closed Loop Results", Proceedings of the 1997 American Control Conference, Albuquerque, NM, June, 1997.

Hasha, M. D., "Reaction Wheel Mechanical Noise Variations," *LMSC EM SSS 218, 1986.*